Kabir, I. R., Yin, D. & Naher, S. (2016). Two dimensional finite element thermal model of laser surface glazing for H13 tool steel. AIP Conference Proceedings, 1769(1), p. 110003. doi: 10.1063/1.4963512

Two Dimensional Finite Element Thermal Model of Laser Surface Glazing for H13 Tool Steel

I. R. Kabir[a)], D. Yin[b)], and S. Naher[c)]

[a,b,c)]Department of Mechanical Engineering and Aeronautics, City University London, EC1V 0HB, United Kingdom,
[b)]Department of Material Processing Engineering, Henan University of Science and Technology, 263 Kaiyuan Avenue, Luoang, China

Corresponding author: [a)]isratrumana@gmail.com
[b)]yindanqing@hotmail.com, [c)]drsumsun.naher@gmail.com

Abstract. A two dimensional (2D) transient thermal model with line-heat-source was developed by Finite Element Method (FEM) for laser surface glazing of H13 tool steel using commercial software-ANSYS 15. The geometry of the model was taken as a transverse circular cross-section of cylindrical specimen. Two different power levels (300W, 200W) were used with 0.2mm width of laser beam and 0.15ms exposure time. Temperature distribution, heating and cooling rates, and the dimensions of modified surface were analysed. The maximum temperatures achieved were 2532K (2259°C) and 1592K (1319°C) for laser power 300W and 200W respectively. The maximum cooling rates were 4.2×10^7 K/s for 300W and 2×10^7 K/s for 200W. Depths of modified zone increased with increasing laser power. From this analysis, it can be predicted that for 0.2mm beam width and 0.15ms time exposer melting temperature of H13 tool steel is achieved within 200-300W power range of laser beam in laser surface glazing.

1. INTRODUCTION

Hot worked tool steel like H13 tool steel is widely used in casting industry as die casting tool. In order to increase die life, surface treatment for enhancing surface properties (hardness, wear, fatigue) is essential [1-6]. In this respect, laser surface glazing (LSG) is an advanced and efficient technique, which offers the best surface properties by creating thin, hard and amorphous layer from the same material. For localized surface treatment, with complex geometry LSG offers best performance without degradation of bulk properties of the specimen. This is used in surface treatment and repairing in aeronautics, automotive, bio implants applications as well [5]. In order to implement LSG process effectively, thermal modeling helps to perceive the relations between thermo-metallurgical features such as temperature distributions, heating and cooling rates, phase transformations, surface properties [2-9]. Although, some FEM modelling for other laser surface treatments was carried out to predict temperature distribution and optimize laser parameters, but laser glazing for H13 tool steel remained nearly untouched [9-13]. One thermal model of LSG for H13 tool steel was done using point heat source of pulse CO_2 laser beam. The model based on analytical temperature model of laser melting process predicted nominal temperatures distribution, depth of molten layer and heating and cooling rate [5, 6]. Some analytical modelling was done to predict melt pool geometry of LSG for ceramic materials [7, 8].

In this work, a FEM 2D thermal modelling was carried out for LSG of H13 tool steel. The aim of doing FEM thermal model was to analyse exact thermal profile using experimental values of the parameters of LSG for H13 tool steel. The thermal analysis generated from this FEM model will help to understand detail heat transfer effects of high density of laser heat source on materials and optimise the process parameters to attain desirable surface

properties (hardness, wear resistance, fatigue, etc.). This model can predict the change in maximum temperature with different laser power levels, beam width and exposure time during the LSG process. Depth of treated zone and heating and cooling rates was also analyzed.

2. MODEL AND METHODOLOGY

The simple cross-section of the cylindrical specimen having 10mm diameter was taken for 2D thermal model. Laser beam was considered as a line heat source that means the laser heat flux irradiated over a line instead of a point on surface. The schematic representation of 2D model is illustrated in Fig. 1(a). The beam was irradiated at a perticular point on the circumference and then moved around it so that beam could treat the whole surface. Due to the line heat source, a molten puddle of half circular shape is created.

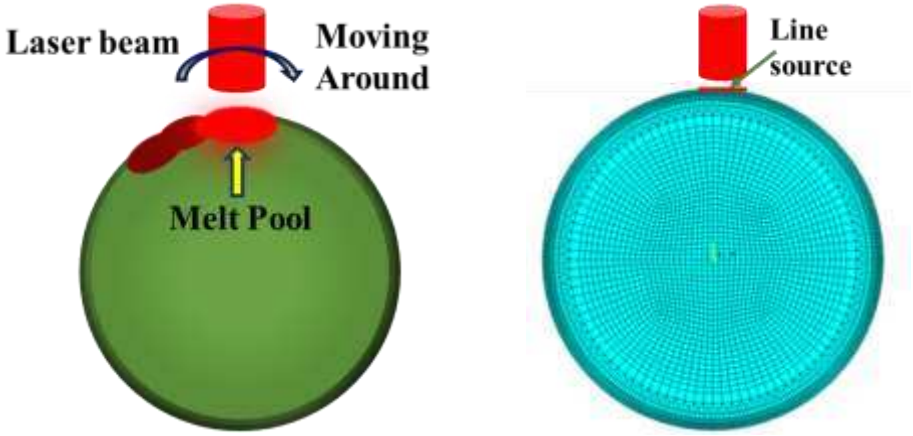

FIGURE 1. (a) Schematic view of 2D cross-section of cylindrical sample with laser beam (b) Meshed cross-sectional area of the model

The element type set for 2D thermal model was PLANE 55. PLANE 55 has 4 nodes with single degree of freedom which is temperature. Transitional meshing technique was followed to mesh the model in order to reduce numbers of nodes and simulation time. The region near the circumference was finely meshed so that the thermal effects on surface due to laser irradiance could be analyzed more accurately. The rest of the part was kept with coarse mesh to reduce simulation time as depicted in Fig. 1(b). The total number of nodes in this model was 6673. The thermo-physical properties of H13 tool steel used in the model can be found in table 1. Physical properties above 2000 °C were kept constant. From table 1 it is obvious that the change in thermo-physical properties are very small after melting temperature (1454 °C). The data extrapolated from these values for each physical property did not have significant effect on surface temperature in this work.

TABLE 1. Thermo-physical properties of H13 tool steel as a function of temperature [8]

Temperature (°C)	**Thermal conductivity ($W\ m^{-1}\ K^{-1}$)**	**Specific Heat ($J\ kg^{-1}K^{-1}$)**	**Density ($kg\ m^{-3}$)**
25	28.6	447	7650
100	29.5	453	7650
500	35.39	519	7640
600	37.09	537	7550
1200	47.29	642	7100
1400	50.69	677	7000
1600	24.06	708	7000
2000	25	721	6900

The thermal model was solved as a transient analysis with time step size taken as 1×10^{-6} seconds. The initial temperature was set up to 20°C as ambient temperature before starting the process, when time t=0. The boundary condition at which laser heat flux was set up at particular region over the surface using Eqs. (1).

$$\nabla(-k\nabla T) = Q_{laser} \tag{1}$$

In Eqs. (1), k denotes thermal conductivity of the material, Q_{laser} is laser heat flux from laser beam and ∇ is the vector operator. The heat loss due to convection and radiation of the laser beam was ignored. The heat input Q_{laser} followed the Eqs. (2).

$$Q_{laser} = \frac{\alpha P_{laser}}{\pi r_0} \exp^{\left(-\frac{2r^2}{r_0^2}\right)} \tag{2}$$

In Eqs. (2), P_{laser} is power of laser beam, r_0 is the laser beam radius, α is the absorption coefficient of material for laser light. The value of α for H13 tool steel was taken 0.3 from a previous study as the absorption of laser light is very poor for this material [5].

3. RESULTS & DISCUSSION

Temperature distribution analysis from the thermal model after LSG helps to understand how much maximum temperature achieved and the gradient of temperature over thickness. Thus it can predict the heat affected region due to laser heat. Fig.2 shows the temperature distributions after heating for two different power levels of continuous laser heat source. The highest temperature for power 300W is 2532K (2259°C) which is 796K higher than the melting point (1727K/1454°C) of H13 tool steel. On the other hand, for 200W laser power the highest temperature is 1597K (1324°C) which is 130K lower than the melting point. From this distribution it can be understood that with decreasing laser power from 300W to 200W the maximum temperature decreases from 2532K to 1597K. Moreover, the optimised power level to reach melting point of LSG of H13 tool steel should be above 200W for 0.15ms exposure time and 0.2mm beam spot size. In the previous experimental study it is also claimed that for 249W average power melting temperature has been attained for LSG of H13 tool steel [2].

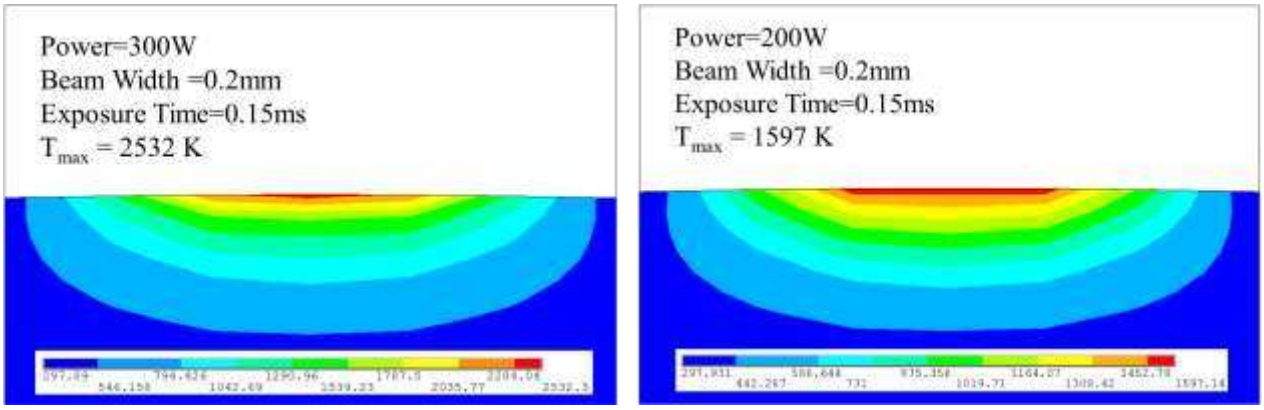

(a) (b)

FIGURE 2. Temperature distribution after heating for 0.15ms (a) power 300W and (b) power 200W

Thermal cycle of heating and cooling was analyzed for two different levels of laser power. Heating and cooling rates predict phase transformation and the level of distortion of the materials. Time-temperature diagram after heating and cooling for 300W and 200W is showing in Fig. 3(a) and 3(b) correspondingly. In these figures, A (on surface), B (15μm) and C (22.5μm) represent heating and cooling curves at different depths from the surface. In Fig 3(a), the peak temperatures found for A B and C are 2532K, 1745K and 1431K respectively for 300W. For 200W, the peak temperatures are 1592K, 1353K, and 1145K for A, B, and C. The heating and cooling rates calculated from these graphs is mentioned in table 2. It is observed that, heating rate increases from 9×10^6 K/s to 1×10^7 K/s with increasing laser power from 200W to 300W. The cooling rates also increases from 2×10^7 K/s to 4.2×10^7 K/s for increasing laser power 200W to 300W. Therefore, a relation between cooling rate and undercooling, ΔT, can be developed form this table. Undercooling is the difference between start temperature and end temperature of cooling.

Higher peak temperature after heating gives greater undercooling and greater undercooling results in higher cooling rate. Hence, the cooling rate for 300W is higher than 200W. Furthermore, the critical isothermal temperature lines Ac_1 (Austenitic starts), Ac_3 (Austenitic finish) and M_s (Martensitic starts) from TTT diagram of H13 tool steel has been superimposed on heating and cooling curves in Figs. 3(a) and 3(b) to predict phase formed after laser glazing process [11]. The calculated cooling rates for both powers are much greater than the critical cooling rate of martensitic transformation for H13 steel [2, 12]. Therefore, it can be predicted that soft phases like ferrite or pearlite cannot form through the modified layer in LSG of H13 steel.

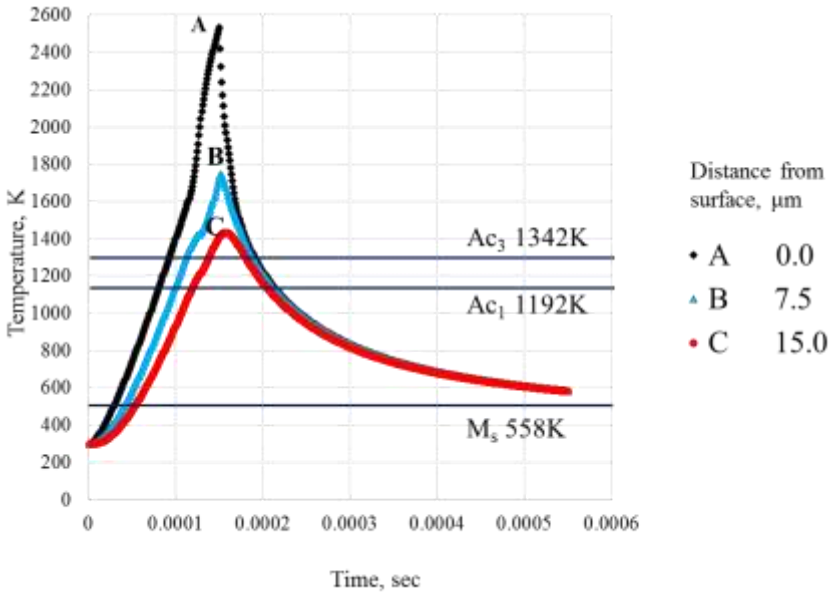

(a)

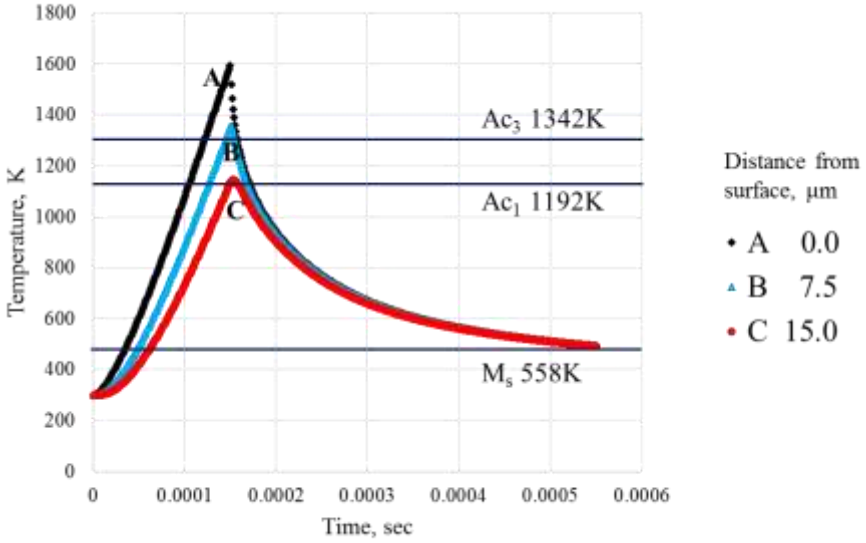

(b)

FIGURE 3. Thermal Cycle (Heating and Cooling rate) at different depth from surface; (a) power 300W and (b) power 200W

TABLE 2. Heating and cooling rate on surface (A curves, Fig. 4a and 4b) for different power

Power	300W	200W
Rate of Heating, K/s	1×10^7	9×10^6
Maximum Rate of Cooling, K/s	4.2×10^7	2×10^7
	(Temp range, K: 2532-1566)	(Temp range, K: 1593-1148)

The depth of modified layer is correlated with temperature distribution in LSG. The area having temperature above the melting point (1727K) was considered as molten zone. Similarly, heat affected zone (HAZ) was accounted from temperature below melting point upto 790K where significant change in phases occurs. Figure 4(a) and 4(b) shows the depth of modified zone due to the laser irradiation at 300W and 200W power respectively. For, power 300W, the depth of melting zone is 7.5µm and that of for HAZ is 30µm, see Fig. 4(a). In Fig. 4(b), only HAZ having depth 30µm was found because temperature did not exceed upto melting point for power 200W. Therefore, depth of modified layer increased with increase on power level. The previous experimental study of LSG of H13 tool steel also showed that depth of modified zone increases with increasing laser power level [2].

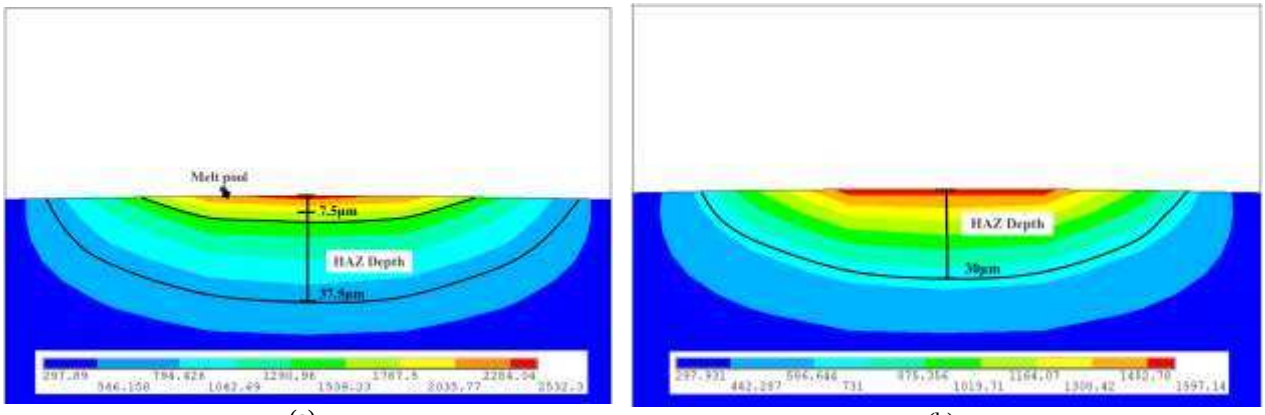

(a) (b)

FIGURE 4. Depth of melt pool and heat affected zone (HAZ) (a) power 300W and (b) power 200W

4. CONCLUSIONS

The 2D transient thermal model of laser surface glazing with line heat source was successfully developed. The model predicted thermal distribution for H13 tool steel at power 200W and 300W for beam width of 0.2 mm and exposure time 0.15ms. The maximum temperature found (2532K) for 300W laser power was above melting point (1727K) of H13 tool steel. For 200W, maximum temperature (1597K) did not reach to melting point. The heating and cooling rates increased with increasing laser power. The depth of heat treated area calculated from the model was 1.25 times greater for 300W (37.5µm) than 200W (30µm). A small molten layer of 7.5µm depth was found for 300W. From this prediction, it is clear that the power level should be above 200W during LSG of H13 tool steel. The developed thermal model can be further utilized to predict residual thermal stress, phase transformations and properties of modified surface layer of LSG.

ACKNOWLEDGMENTS

The work described in this paper has been supported by INTACT project of Erasmus-Mundus (Grant agreement reference: 2013-2829/001-001-EM Action2-Partnerships), and Department of Mechanical Engineering and Aeronautics of City University London. The author would be grateful enough to Dr. Ranjan Banerjee, Professor of Structural Dynamics in City University London, for his valuable guidance in developing the FEM thermal model.

REFERENCES

1. B. H. Kear, E. M. Breinan, and L. E. Greenwald, Met. Technol., **April**, pp. 121–129 (1979).
2. S. N. Aqida, S. Naher, M. Maurel, and D. Brabazon, in 25th International Manufacturing Conference, 3-5 Sept 2008, Dublin, Ireland.
3. S. N. Aqida, S. Naher, and D. Brabazon, in AIP Conference Proceedings, **1353**, pp. 1081–1086 (2011).
4. E. Chikarakara, S. Naher, and D. Brabazon, Appl. Phys. A Mater. Sci. Process., **101**, pp. 367–371 (2010).
5. S. N. Aqida, S. Naher, and D. Brabazon, Key Eng. Mater., **504–506**, pp. 351–356 (2012).
6. A. Issa, D. Brabazon, and M. S. J. Hashmi, J. Mater. Process. Technol., **207**, pp. 307–314 (2008).
7. A. Peligrad, E. Zhou, D. Morton, and L. Li, Opt. Laser Technol., **33**, pp. 7–13 (2001).
8. L. Hao and J. Lawrence, J. Mater. Process. Technol., **180**, pp. 110–116 (2006).
9. M. J. Tobar, C. Álvarez, J. M. Amado, A. Ramil, E. Saavedra, and A. Yáñez, Surf. Coatings Technol., **200**, pp. 6362–6367 (2006).
10. M. Hao and Y. Sun, Int. J. Heat Mass Transf., **64**, pp. 352–360 (2013).
11. S. Santhanakrishnan, F. Kong, and R. Kovacevic, J. Mater. Process. Technol., vol. **211**, pp. 1247–1259 (2011).
12. P. Farahmand, P. Balu, F. Kong, and R. Kovacevic, in ASME 2013 International Mechanical Engineering Congress and Exposition, pp. 1–12, 2015.
13. K. M. Mchugh, Y. Lin, and Zhou, Y, and E. J. Lavernia, Mater. Sci. Eng. A, **477**, pp. 50–57 (2008).

APPENDIX

Calculation of heating and cooling rates

The heating and cooling rate was calculated from the time-temperature plot in Fig. 4(a) and 4(b). In Fig. 4(a) and 4(b), temperature was plotted along Y axis and time was plotted along X axis. For calculating the rates of heating and cooling the difference of temperature was divided by the difference of time. If the temperature difference would be ΔT, and heating or cooling time would be t, then the rate, R would be as mentioned in Eqs. 3.

$$R = \frac{\Delta T}{t} \tag{3}$$